# The Mechanism of Allosteric Coupling in Choline Kinase α1 Revealed by the Action of a Rationally Designed Inhibitor**

*María Sahún-Roncero, Belén Rubio-Ruiz, Giorgio Saladino, Ana Conejo-García, Antonio Espinosa, Adrián Velázquez-Campoy, Francesco Luigi Gervasio, Antonio Entrena, and Ramon Hurtado-Guerrero**

Choline kinase (CHOK) is a homodimeric enzyme that catalyzes the transfer of a phosphate group from ATP to choline to produce ADP and phosphocholine (PCho; Figure 1 A), the first step in the Kennedy pathway leading to the synthesis of phosphatidylcholine (PtdCho).[1] An overexpression of the α isoform of CHOK has been associated with human cancers because PtdCho is required for the growth of cancer cells.[2] These findings have motivated the development of CHOKα inhibitors, such as hemicholinium-3 (HC-3; Figure 1 B),[3] and a large number of HC-3 derivatives.[4,5] Although early studies reported evidence of cooperative binding in CHOK,[6] the binding of HC-3 does not involve allosteric coupling between the two monomers. We recently synthesized a new family of monocationic CHOK inhibitors that, in contrast to HC-3, are non-symmetrical.[7] Herein, we characterized one of these compounds (compound 1; Figure 1 B and Supporting Information, Table S1) and found evidence of a significant allosteric coupling between the two monomers characterized by negative cooperativity and a broken symmetry.

Allostery is the process whereby the binding of a ligand to a biological macromolecule (protein) induces an effect on a distant functional site. Two classical models have been proposed to describe allostery: the Monod–Wyman–Changeaux (MWC) or concerted model[8] and the sequential model.[9] The first posits that the conformational changes in the different monomers of the bio-macromolecule are strongly coupled and that symmetry is conserved among the mono-

mers. The second assumes a strong coupling between binding and conformational changes. More recently molecular dynamics simulations helped in linking large-amplitude motions to allosteric mechanisms[10] and an ensemble view of allostery has been proposed, reconciling multiple protein conformations with allosteric signaling.[11] Herein, by using a combination of experimental (isothermal titration calorimetry (ITC), X-ray crystallography) and computational approaches, we observed a broken inter-monomer symmetry leading to negative cooperativity and a dynamic recovery of the symmetry owing to a fast inter-conversion of conformers.

Compound 1 (Figure 1 B) has a 4-substituted pyridinium and an adenine moiety connected by a flexible linker.[7] Its adenine moiety docks to the ATP site of the enzyme, while the pyridinium fragment occupies the choline binding site. In stark contrast to HC-3, 1 induces negative cooperativity. It exhibits the expected biphasic titration curves and a cooperativity constant $\alpha$ of 0.2, corresponding to a cooperativity $\Delta G$ of 0.95 kcal mol$^{-1}$ and a Hill coefficient of 0.62 (Figure 1 C, Table S1 and Supporting Information). Compound 1 first binds to one monomer of the dimeric CHOKα1 with a dissociation constant $K_{d1}$ of 38 nM. The binding to one monomer induces negative cooperativity on the second monomer, leading to a higher $K_{d2}$ of 190 nM (Table S1). An allosteric coupling between the two monomers has been reported in *S. cerevisiae* CHOK (*Sc*CHOK) where positive cooperativity upon ATP binding was observed.[6b] We also checked in CHOKα1 whether AMP-PNP, an analogue of

---

[*] M. Sahún-Roncero, Dr. A. Velázquez-Campoy,
Dr. R. Hurtado-Guerrero
Institute of Biocomputation and Physics of Complex Systems (BIFI),
University of Zaragoza,
BIFI-IQFR (CSIC) Joint Unit, Mariano Esquillor s/n, Campus Rio
Ebro, Edificio I + D; Fundacion ARAID
Edificio Pignatelli 36 (Spain)
E-mail: rhurtado@bifi.es

Dr. B. Rubio-Ruiz, Dr. A. Conejo-García, Prof. A. Espinosa,
Prof. A. Entrena[+]
Departamento de Química Farmacéutica y Orgánica, Facultad de
Farmacia, Universidad de Granada
c/Campus de Cartuja s/n, Granada (Spain)

Dr. G. Saladino, Dr. F. L. Gervasio[+]
Computational Biophysics group,
Spanish National Cancer Research Center
Melchor Fernández Almagro, 3, Madrid (Spain)
and
Department of Chemistry, University College London
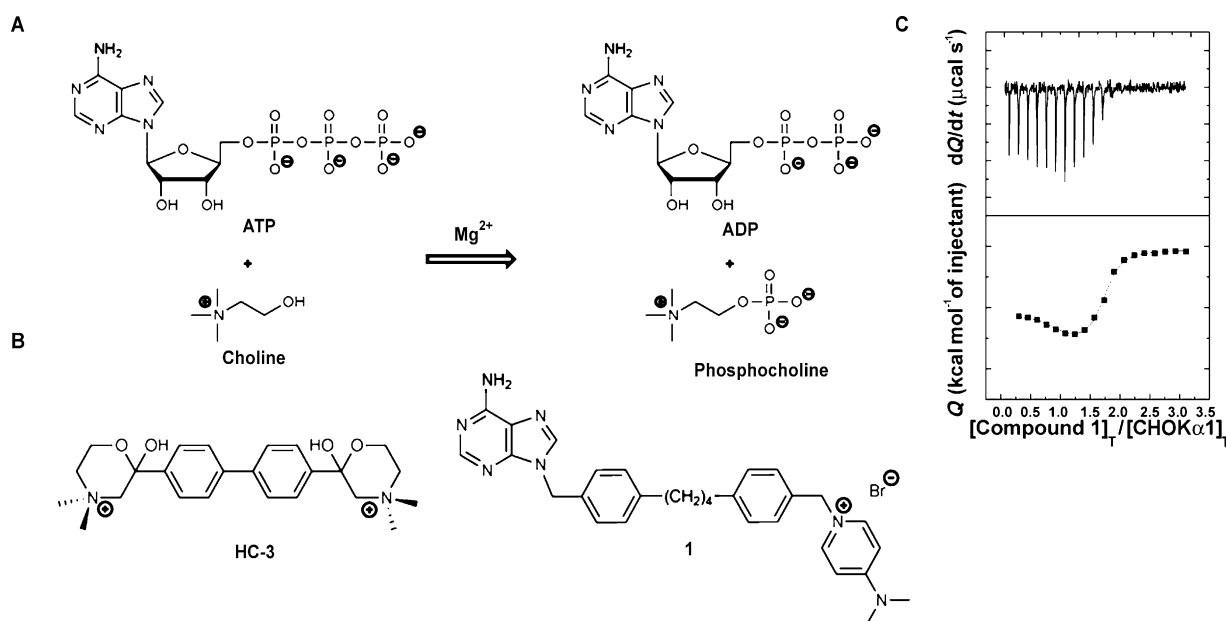20 Gordon Street, London WC1H 0AJ (UK)

**Figure 1.** Biophysical characterization of compound **1**. A) Scheme of the CHOK enzymatic reaction. B) Chemical formulas of **1** and HC-3. C) ITC data for the binding of **1** to CHOKα1. Top: Raw thermogram (thermal power versus time). Bottom: Binding isotherm (normalized heats versus molar ratio). See Table S1 for the thermodynamic and $K_d$ values for **1** and HC-3.

ATP, shows cooperativity effects, but we did not find any (Table S1), suggesting that **1** induces negative cooperativity by binding in a different manner with respect to ATP.

To test this hypothesis, we solved the crystal structure of CHOKα1-**1** at 1.90 Å resolution (Table S2), using molecular replacement using a template (PDB ID: 3G15; see Supporting Information).[3a] Successive iterative model building and refinement cycles were carried out to produce final models with good refinement statistics (Table S2). The structure is a dimer in which each monomer is formed by a small N-terminal domain that binds ATP and a large C-terminal domain that binds choline (Figure 2A). Whereas the ATP binding site is located in a cleft formed by the N- and C-

terminal residues, the choline binding site is found in a deep hydrophobic pocket.[12] In agreement with docking predictions,[7] **1** fully occupies the 20 Å long active site, from the ATP to the choline binding sites, explaining its potency (Figure 2A and Figure 3A,B). The main interactions between **1** and CHOKα1 are illustrated in Figure S1.

A comparison of the overall CHOKα1-**1** crystal structure with the apo structure (PDB ID: 2CKO)[12] revealed large conformational changes (Figure 2B). To ensure that crystal packing did not play a role in determining the conformational states, we only used crystal structures sharing the same space group, similar unit cell dimensions, and crystal packing (Table S3). The extent of opening of the binding sites of
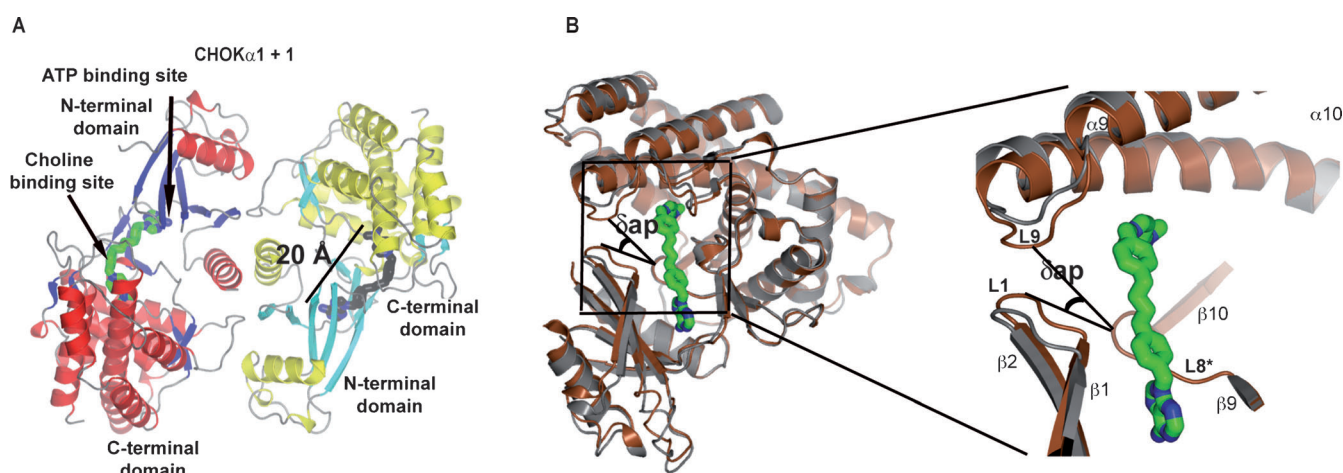


**Figure 2.** Overall structure of CHOKα1-**1** and conformational states of CHOKα enzymes. A) Overall crystal structure of CHOKα1 in complex with **1**. Secondary structure elements from the CHOKα1 structure are shown, with α-helices in red (monomer A) and yellow (monomer B), and β-strands respectively in blue and cyan. **1** is shown as a stick model with green and black carbon atoms. B) Illustration of how aperture angle ($\delta_{ap}$) is calculated. Monomer B of CHOKα1-**1** structure (brown) is superimposed on monomer B of the apo structure (gray).

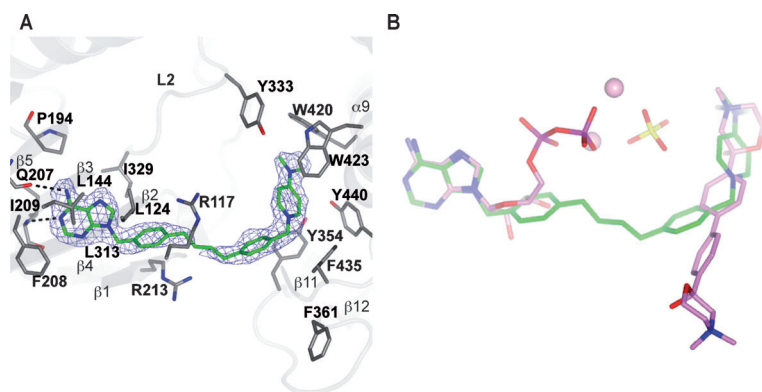**Figure 3.** Active site of CHOKα1 in complex with compound **1**. A) Active site of CHOKα1 in complex with **1**. Amino acids in the active site are shown as stick models with gray carbon atoms. **1** is shown as a stick model with green carbon atoms. Protein-ligand hydrogen bonds are dotted black lines. Unbiased difference electron density maps are shown at 2.2 σ. B) Superimposition of CHOKα1s structures in complexes with **1** (green carbon atoms) and ADP/HC-3 (pink carbon atoms).

CHOKα was assessed by measuring the angle $\delta_{ap}$ (Figure 2B) defined by the alpha carbon atom of three residues (Ser121 on loop L1, Glu332 on L8*, and Ser431 on L9) in different structures. The loops, L1 and L9 undergo significant conformational changes and the angle they make with L8*, which is relatively rigid, is able to monitor those changes. The value of $\delta_{ap}$ combined with the root mean square deviations (RMSD) of equivalent alpha carbon atoms from the apo structure (PDB ID: 2CKO) allowed for the identification of three distinct conformational states: open/semi-open, closed, and super-closed states (Figure S2A,B). Open/semi-open states were present in monomers of the apo CHOKα2, CHOKα1-HC-3 (PDB ID: 3F2R), CHOKα1-HC-3-ADP (PDB ID: 3G15), and monomer A of CHOKα1-1; a closed state was present in monomer B of CHOKα1-1; and a super-closed state was present in CHOKα1-PCho (PDB ID: 2CKQ; Figure S2A). The closed and super-closed states followed a trend in which higher RMSD values were associated with a smaller $\delta_{ap}$. The crystal structure of the complex with **1** is asymmetric. Monomer B of the CHOKα1-1 complex differs significantly from monomer A or B of the apo structure, as indicated from an RMSD of 0.9 Å and 1.08 Å, respectively (Figure S2B), and it is significantly different from monomer A present in CHOKα1-1 (RMSD of 1.03 Å; Figure S2B and Figure S3). Owing to differences in the position of the loops at the cavity entrance, the entrance to the cavity and its size are different (loops L1 and L9, see Figure 2B), hinting at possible allosteric couplings between the two monomers. This striking asymmetry could provide the structural basis of the negative cooperativity, as proposed by Levitzki et al.[13] (Figure S2,S3).

To further explore the origin of the negative cooperativity and verify the long-range couplings, we performed extensive computational modeling with two complementary methods: all-atom molecular dynamics (MD) simulations and anisotropic elastic network model (ENM).[14] All-atom MD with an explicit solvent can accurately reproduce local and large-scale conformational changes.[15] However, long-MD simulations

are computationally expensive and the time scales that can be effectively sampled are often insufficient to gather statistically meaningful data on long-range conformational changes. ENMs are based on coarser approximations. The protein is represented by a subset of atoms (often the alpha carbon atom, Cα) interconnected by a network of elastic springs. Although this model is much simpler with respect to MD, its normal modes are representative of the motions of the protein around its crystallographic structure.

We first performed an analysis based on the perturbation of an anisotropic ENM.[14] The analysis consists of moving the Cα atoms around atom *i* along each normal mode, giving rise to a new distorted structure. If the structures arising from moving the Cα atoms around atom *j* along the same eigenvectors are distorted in a correlated way, *i* and *j* are allosterically coupled in the structure. The ENM analysis confirms the existence of an allosteric network connecting the two monomers (Figure S4). Many distant elements, far from the interface, showed a non-trivial allosteric coupling (Figure S4, Figure 4A). The strongest coupling was found between the two α7 helices, which are far from the interface. The α7 helix was also coupled with the two long α9 helices of the other monomer (e.g. α9 of monomer A was coupled with α7 of monomer B and vice versa; Figure S4, Figure 4A). The α9 helices are involved in the opening of the cavity. Finally, the α7 helices in monomers A and B are coupled to the interfacial motifs α2, β4, and β5, with less intense couplings observed also between α9 and the α2β4β5 region (Figure S4, Figure 4A). Thus, there is a coupling between the dimer interface (α2β4β5) and the choline binding pocket. The allosteric signal flows from the dimer interface to loop L9, involved in the opening/closing mechanism, through helix α7. Because this model involves the perturbation of a specific crystal structure, it is sensitive to the conformation (apo or holo) used for the analysis. Interestingly, some α7 residues are part of the choline binding site and interact with compound **1** directly. However, no differences were observed in the choline binding site of the two monomers. Instead, significant differences were observed at the other end of the ligand, the adenine moiety that binds in the kinase ATP binding site. Indeed, in the monomer B, which is more closed and to which **1** binds better, the ligand makes stronger (shorter length) hydrogen bonds to Gln207 and Ile209 (Figure 3A). Based on these observations, it seems unlikely that the binding of the first molecule directly triggers the closure of the L1–L9 loops. Instead, the stronger binding of **1** to the ATP binding site, and in particular to the hinge region preceding β4 and β5, might be responsible for both the L1–L9 loops closure and the perturbation of the other monomer binding site, through the coupling with α7 (Figure 4A).

To verify the coupling between different structural elements in the CHOKα1 dimer and to investigate the driving force for L1–L9 loop closure and the break of symmetry, we performed fully atomistic MD. The MD simulations in an explicit solvent were performed with
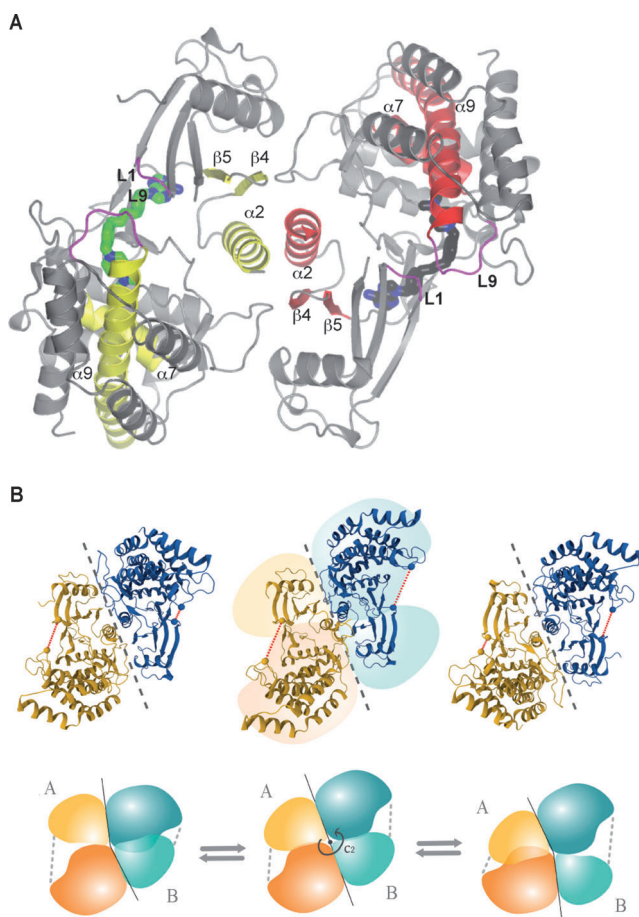
© 2013 Wiley-VCH Verlag GmbH & Co. KGaA, Weinheim

**Figure 4.** Elastic network analysis and molecular dynamics simulations. A) Overall structure of CHOKα1 showing the coupled secondary structures and the L1 and L9 loops (see also Figure S4, S5 for the numbering of secondary structures and loops). B) Scheme demonstrating that during the simulation, the protein dimer shifts from a closed conformation of monomer B to a final conformation where monomer A is closed.

original binding pocket of monomer A contained more water molecules ($150 \pm 1$ in a 5 Å solvation shell around the ligand) compared to monomer B ($98 \pm 1$; Figure S6). Owing to the insertion of water between the pyridinium end and the hydrophobic residues Tyr333, Tyr354, Trp420, and Trp423, large fluctuations of the ligand are observed at the choline binding site when the pocket is in the open conformation. This explains the higher affinity of **1** to the closed conformation that is initially assumed by monomer B (Figure S6). To confirm the allosteric coupling of the two monomers, we performed a second set of simulations. We removed the ligand bound to the most favorable A*B conformation and let the system relax for more than 50 ns. In the simulation, we observed a very fast shift towards the opposite AB* conformation, thus supporting the tight allosteric coupling between the two active site pockets (Figure S7). To optimize the interactions between the ligand and the hydrophobic residues in the choline binding site, monomer A* rapidly assumes a closed conformation which leads to the opening of monomer B. Principal component analysis (PCA) revealed that the closure of L1/L9 triggers the sliding of helix α2 and β4β5. These are engaged in inter-monomer protein–protein interactions and cause an opposite movement of the N-lobe of monomer A, leading to the opening of its cavity.

The tight coupling between the monomers through the α2β4β5-α7-α9-L9 elements explain the origin of the negative/positive cooperativity reported previously for CHOK from different species.[6] More importantly, our simulations show that the broken symmetry observed in the crystal structure can be dynamically recovered on average because of the fast exchange of the closed and open states assumed by the monomers.

In conclusion, we have investigated the binding mechanism of a compound that induces a negative-cooperativity allosteric mechanism in CHOKα1 with a break of the dimer symmetry. We determined by protein X-ray crystallography that not only is a large conformational change induced by compound **1**, but also that the conformation assumed by the two bound monomers are dissimilar. The consequent asymmetry of the dimer could explain the negative cooperativity, as was first proposed by Levitzki et al.[13] and recently observed in the EGF receptor[20] and human hemoglobin.[21] However, MD simulations showed that the two monomers, coupled through the α2β4β5-α7-α9-L9 motifs, alternatively assume an open/semi-open or closed state with a fast inter-conversion rate, recovering on average the symmetry proposed in the original MWC model. Taken together, our data explain the molecular mechanism of the negative cooperativity, the inter-monomer coupling, and sets the foundation to design better and more selective inhibitors.

GROMACS 4.5[16] using the Amber99SB*-ILDN[17] force field for the protein part and GAFF[18] for the ligand. The system was solvated with 35 378 water molecules in a dodecahedral box and neutralized with two Na$^+$ ions (see Supporting Information). A 300 ns MD simulation of the dimer bound to two molecules of **1** was run to characterize the differences in the binding of the molecule to the two monomers and rationalize their different $K_d$s. The inter-conversion of the two monomer conformations was very fast (100 ns time scale). Fast hinge-bending motions in the 1–100 ns time scale have been reported previously,[10a,c] also in other kinases.[19] Starting from a conformation where the monomer A is open (A*) and the monomer B is closed (B), a transition to an opposite conformation AB*, where the second monomer is open, was observed after approximately 70 ns. After another 100 ns, the dimer went back to the original A*B conformation (Figure 4B). Initially, the two hydrogen bonds between **1** and the binding pocket of the open monomer A were less populated (48% with Gln207 and 58% with Ile209) than those of the closed monomer B (75% and 83%, respectively). The

[1] K. Glunde, Z. M. Bhujwalla, S. M. Ronen, *Nat. Rev. Cancer* **2011**, *11*, 835–848.

[2] A. Yalcin, B. Clem, S. Makoni, A. Clem, K. Nelson, J. Thornburg, D. Siow, A. N. Lane, S. E. Brock, U. Goswami, J. W. Eaton, S. Telang, J. Chesney, *Oncogene* **2010**, *29*, 139–149.

[3] a) B. S. Hong, A. Allali-Hassani, W. Tempel, P. J. Finerty, Jr., F. Mackenzie, S. Dimov, M. Vedadi, H. W. Park, *J. Biol. Chem.* **2010**, *285*, 16330–16340; b) F. W. Schueler, *J. Pharmacol. Exp. Ther.* **1955**, *115*, 127–143; c) J. G. Cannon, *Med. Res. Rev.* **1994**, *14*, 505–531.

[4] a) J. M. Campos, R. M. Sanchez-Martin, A. Conejo-Garcia, A. Entrena, M. A. Gallo, A. Espinosa, *Curr. Med. Chem.* **2006**, *13*, 1231–1248; b) D. Gallego-Ortega, T. Gomez del Pulgar, F. Valdes-Mora, A. Cebrian, J. C. Lacal, *Adv. Enzyme Regul.* **2011**, *51*, 183–194; c) D. Gallego-Ortega, A. Ramirez de Molina, M. A. Ramos, F. Valdes-Mora, M. G. Barderas, J. Sarmentero-Estrada, J. C. Lacal, *PLoS One* **2009**, *4*, e7819.

[5] a) A. Rodríguez-González, A. Ramirez de Molina, F. Fernandez, M. A. Ramos, M. del Carmen Nunez, J. Campos, J. C. Lacal, *Oncogene* **2003**, *22*, 8803–8812; b) A. Rodriguez-Gonzalez, A. Ramirez de Molina, J. Benitez-Rajal, J. C. Lacal, *Prog. Cell Cycle Res.* **2003**, *5*, 191–201; c) N. M. Al-Saffar, H. Troy, A. Ramirez de Molina, L. E. Jackson, B. Madhu, J. R. Griffiths, M. O. Leach, P. Workman, J. C. Lacal, I. R. Judson, Y. L. Chung, *Cancer Res.* **2006**, *66*, 427–434; d) A. Rodríguez-González, A. Ramirez de Molina, F. Fernandez, J. C. Lacal, *Oncogene* **2004**, *23*, 8247–8259.

[6] a) M. A. Brostrom, E. T. Browning, *J. Biol. Chem.* **1973**, *248*, 2364–2371; b) K. H. Kim, D. R. Voelker, M. T. Flocco, G. M. Carman, *J. Biol. Chem.* **1998**, *273*, 6844–6852.

[7] B. Rubio-Ruíz, A. Conejo-Garcia, P. Rios-Marco, M. P. Carrasco-Jimenez, J. Segovia, C. Marco, M. A. Gallo, A. Espinosa, A. Entrena, *Eur. J. Med. Chem.* **2012**, *50*, 154–162.

[8] J. P. Changeux, *Annu. Rev. Biophys.* **2012**, *41*, 103–133.

[9] D. E. Koshland, Jr., G. Nemethy, D. Filmer, *Biochemistry* **1966**, *5*, 365–385.

[10] a) B. L. de Groot, G. Vriend, H. J. Berendsen, *J. Mol. Biol.* **1999**, *286*, 1241–1249; b) J. Ma, P. B. Sigler, Z. Xu, M. Karplus, *J. Mol. Biol.* **2000**, *302*, 303–313; c) R. Baron, N. A. Vellore, *Proc. Natl. Acad. Sci. USA* **2012**, *109*, 12509–12514.

[11] F. Bai, R. W. Branch, D. V. Nicolau, Jr., T. Pilizota, B. C. Steel, P. K. Maini, R. M. Berry, *Science* **2010**, *327*, 685–689.

[12] E. Malito, N. Sekulic, W. C. Too, M. Konrad, A. Lavie, *J. Mol. Biol.* **2006**, *364*, 136–151.

[13] A. Levitzki, W. B. Stallcup, D. E. Koshland, Jr., *Biochemistry* **1971**, *10*, 3371–3378.

[14] I. A. Balabin, W. Yang, D. N. Beratan, *Proc. Natl. Acad. Sci. USA* **2009**, *106*, 14253–14258.

[15] a) G. Saladino, F. L. Gervasio, *Curr. Top. Med. Chem.* **2012**, *12*, 1889–1895; b) P. Maragakis, M. Karplus, *J. Mol. Biol.* **2005**, *352*, 807–822; c) P. C. Whitford, S. Gosavi, J. N. Onuchic, *J. Biol. Chem.* **2008**, *283*, 2042–2048.

[16] B. Hess, C. Kutzner, D. van der Spoel, E. Lindahl, *J. Chem. Theory Comput.* **2008**, *4*, 435–447.

[17] a) K. Lindorff-Larsen, S. Piana, K. Palmo, P. Maragakis, J. L. Klepeis, R. O. Dror, D. E. Shaw, *Proteins Struct. Funct. Genet.* **2010**, *78*, 1950–1958; b) R. B. Best, G. Hummer, *J. Phys. Chem. B* **2009**, *113*, 9004–9015.

[18] J. Wang, R. M. Wolf, J. W. Caldwell, P. A. Kollman, D. A. Case, *J. Comput. Chem.* **2004**, *25*, 1157–1174.

[19] a) Z. Palmai, L. Chaloin, C. Lionne, J. Fidy, D. Perahia, E. Balog, *Proteins Struct. Funct. Genet.* **2009**, *77*, 319–329; b) N. Smolin, R. Biehl, G. R. Kneller, D. Richter, J. C. Smith, *Biophys. J.* **2012**, *102*, 1108–1117.

[20] D. Alvarado, D. E. Klein, M. A. Lemmon, *Cell* **2010**, *142*, 568–579.

[21] G. K. Ackers, J. M. Holt, *J. Biol. Chem.* **2006**, *281*, 11441–11443.